

Optical and electrical properties of Mg-doped AlN nanowires grown by molecular beam epitaxy

Ashfiqua Tahseen Connie,¹ Songrui Zhao,¹ Sharif Md. Sadaf,¹ Ishiang Shih,¹ Zetian Mi,^{1,a)} Xiaozhang Du,² Jingyu Lin,² and Hongxing Jiang²

¹Department of Electrical and Computer Engineering, McGill University, 3480 University Street, Montreal, Quebec H3A 0E9, Canada

²Department of Electrical and Computer Engineering, Texas Tech University, Lubbock, Texas 79409, USA

(Received 15 January 2015; accepted 9 May 2015; published online 26 May 2015)

In this paper, the optical and electrical properties of Mg-doped AlN nanowires are discussed. At room temperature, with the increase of Mg-doping concentration, the Mg-acceptor energy level related optical transition can be clearly measured, which is separated about 0.6 eV from the band-edge transition, consistent with the Mg activation energy in AlN. The electrical conduction measurements indicate an activation energy of 23 meV at 300 K–450 K temperature range, which is significantly smaller than the Mg-ionization energy in AlN, suggesting the p-type conduction being mostly related to hopping conduction. The free hole concentration of AlN:Mg nanowires is estimated to be on the order of 10^{16} cm^{-3} , or higher. © 2015 AIP Publishing LLC. [<http://dx.doi.org/10.1063/1.4921626>]

AlN, with a large direct bandgap of ~ 6.1 eV, extends the group III-nitride semiconductor family into the deep ultraviolet (DUV) spectral range. It also possesses many excellent properties, such as high thermal conductivity, high thermal and chemical stability, large mechanical strength and hardness, and miscibility with GaN.¹ To date, however, the achievement of high performance DUV optoelectronic devices has been largely limited by the extremely poor conductivity of p-type Al(Ga)N, which is directly related to the very large activation energy (~ 0.5 – 0.6 eV) for Mg-dopant in AlN.² In addition, the presence of extensive dislocations and defects in conventional AlN epilayers, including nitrogen (N) vacancies, leads to strong compensation effects.^{3,4} For example, it has been measured that the formation energy for N-vacancies is reduced significantly with increasing Al composition and/or Mg incorporation.⁵

Such critical challenges can be overcome, to a great extent, by employing low dimensional nanostructures, such as nanowire, due to the highly efficient lateral stress relaxation⁶ and the minimized epitaxial relation between the substrate and nanowires.⁷ Previously, the growth/synthesis of Mg-doped AlN nanowires using various techniques, including direct arc discharge method, metal organic chemical vapor deposition (MOCVD), and molecular beam epitaxy (MBE), have been reported.^{8–14} These studies, however, mostly focus on the magnetic properties of Mg-doped AlN nanowires. In addition, such Mg-doped AlN nanowires exhibit poor optical qualities, and band-edge emission was not measured at room temperature. As a consequence, there lacks a detailed understanding of the fundamental electrical and optical properties and their correlation with the various defect states and electrical conduction in Mg-doped AlN nanowires.

Recently, with the use of an improved MBE growth process, we demonstrated strain-free AlN nanowires on Si

substrate that can exhibit strong free-exciton emission at room temperature.¹⁵ In addition, defect bands, including nitrogen vacancy related emission peaks, which were commonly measured in AlN epilayers, were found to be absent in such AlN nanowire structures. Based on such superior quality AlN nanowires, we have also demonstrated AlN nanowire light emitting diodes (LEDs) directly on Si substrate.¹⁶ In this work, we have further performed a detailed study of the MBE growth and characterization of Mg-doped AlN nanowires on Si substrate. Mg-acceptor related optical transition is clearly measured *at room temperature* under optimized growth conditions. Furthermore, the temperature dependent electrical measurements show the presence of different activation energies in different temperature ranges. The low activation energy (~ 23 meV) in 300 K–450 K temperature range indicates that the hole conduction is mainly dominated by hopping conduction at room temperature.

In this work, catalyst-free Mg-doped AlN nanowires were grown on Si-substrate by radio frequency plasma-assisted MBE under nitrogen rich conditions. Prior to the growth of AlN nanowires, GaN nanowire template was first grown on Si(111) substrate, schematically shown in Fig. 1(a), which can promote the formation of AlN nanowires with controlled properties.^{17,18} A series of AlN:Mg nanowire samples were grown and studied,

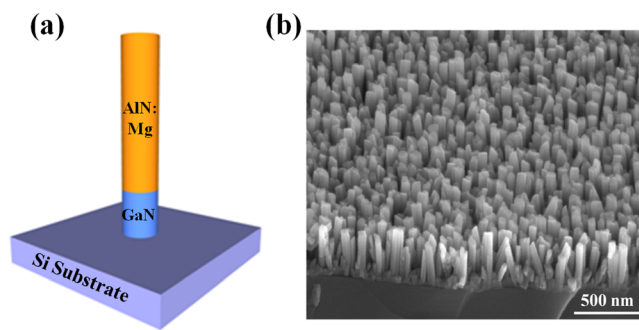


FIG. 1. (a) Schematic diagram of AlN nanowire grown on GaN template on a Si substrate. (b) An SEM image of AlN:Mg nanowires taken with a 45° angle.

^{a)}Author to whom correspondence should be addressed. Electronic mail: zetian.mi@mcgill.ca. Tel.: 1-514-398-7114.

TABLE I. Growth parameters for Mg-doped AlN samples having different growth rates and different doping levels.

Samples	Al-flux (Torr)	Mg-flux (Torr)
A	4.0×10^{-8}	2.6×10^{-9}
B	4.0×10^{-8}	1.6×10^{-8}
C	4.0×10^{-8}	9.1×10^{-8}
D	2.0×10^{-8}	2.6×10^{-9}
E	2.0×10^{-8}	9.1×10^{-8}

listed in Table I. Samples A, B, and C were grown with an Al flux of 4.0×10^{-8} Torr, and Mg flux of 2.6×10^{-9} Torr, 1.6×10^{-8} Torr, and 9.1×10^{-8} Torr, respectively. Samples D and E were grown with Al flux of 2.0×10^{-8} Torr, and Mg flux of 2.6×10^{-9} Torr and 9.1×10^{-8} Torr, respectively. The axial growth rate is ~ 3.5 nm/min for samples A, B, and C, and ~ 1.5 nm/min for samples D and E. For all the samples, the substrate growth temperature was kept at 790 °C, and the nitrogen flow rate was 1 standard cubic centimeter per minute (sccm) with a forward plasma power of 350 W. Figure 1(b) presents the scanning electron microscopy (SEM) image of sample B. It is seen that the nanowires are vertically aligned and exhibit a high degree of size uniformity. The height and density of the nanowires are estimated to be ~ 500 nm and 1×10^{10} cm $^{-2}$, respectively. Our previous studies further confirm that the nanowires are grown along the c-axis.¹⁶

Temperature variable photoluminescence (PL) measurements were performed on as grown Mg-doped AlN nanowires using a 193 nm ArF excimer laser as the excitation source. The emission from the nanowires was spectrally resolved using a high-resolution spectrometer and was detected by a photomultiplier tube (PMT). Figure 2(a) presents the PL spectra of the AlN:Mg nanowires at 20 K. The spectra presents a narrow peak at ~ 205 nm (6.05 eV), and a broad peak at 227.4 nm (5.45 eV) for samples C, D, and E. A variation is observed in the high energy peak positions of the samples, which is due to the change in the growth conditions. The first peak (high energy peak) is denoted as P_H, and the second broad peak is denoted as P_L. P_H is due to the excitons bound to neutral Mg-acceptor impurities (I₁ line in AlN). Various defect related transitions have been identified for planar AlN.^{5,19,20} These defect emissions are mainly due to the nitrogen/cation vacancies and related complexes in AlN. In previously reported AlN:Mg epilayers, the optical transition involving the deep level

donor and Mg-acceptor is observed at 4.7 eV and the transition involving shallow donor and deep acceptor is observed at 3.9 eV.¹⁹ These facts rule out the possibility of the low energy peak at 227.4 nm (5.45 eV) to be a defect peak and, therefore, P_L can be attributed to the donor acceptor pair (DAP) transition between a shallow donor and Mg-acceptor energy level.^{2,21} The ionization energy of the shallow donor derived from the temperature dependent PL studies is ~ 80 meV (discussed later). The ionization energy of the Mg-acceptor (E_0) is further estimated from, $E_0 = E_g - 5.45 - 0.08 = 0.61$ eV, with $E_g = 6.14$ eV being the band gap of AlN at 20 K, which is consistent with the Mg-activation energy in AlN.² This Mg-acceptor related peak increases with Mg-dopant incorporation. Moreover, it is more pronounced for samples D and E, grown with a reduced growth rate (low Al flux), indicating that a slower growth rate significantly enhances Mg-incorporation. This observation is further supported by the comparison between samples A (high Al flux) and D (low Al flux), which were both grown with the same Mg flux of 2.6×10^{-9} Torr. It is seen that no Mg-acceptor related transition can be observed for sample A, whereas such a transition can be clearly measured in sample D. The direct correlation between the emission peak at 227.4 nm with Mg-dopant incorporation provides unambiguous evidence for the presence of Mg-acceptors in AlN. The strong dependence of Mg-dopant concentration on variations of the growth conditions is a result of several competitive processes, including the enhanced Mg-acceptor incorporation due to the reduced formation energy for the Al-substitutional Mg-doping in the near-surface region of nanowires as well as the Mg atom desorption at elevated growth temperature.^{16,22}

The power and temperature dependent PL studies were performed. In what follows, we focus on the highly Mg-doped AlN sample (sample E). The power dependent PL properties at 20 K are shown in Fig. 2(b). The inset of Fig. 2(b) presents the ratio of the peak intensities of Mg-acceptor peak to the band-edge peak. It is observed that the ratio increases in the low power regime but decreases with further increasing excitation power. This is related to the saturation of the Mg-acceptor energy level under high excitation conditions. In addition, the power dependence of the peak energies reveals that both the high energy and low energy peaks undergo a red shift with increasing excitation power. The DAP recombination usually causes a blue shift with increasing power and has been observed in GaN²³ and InN.²⁴ It is

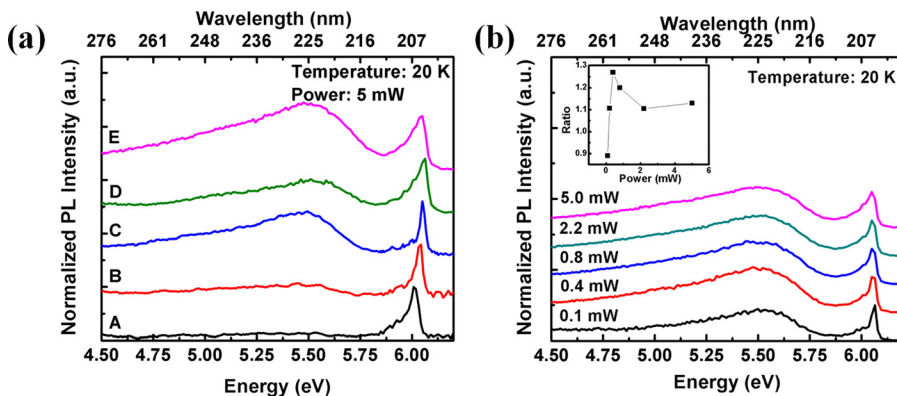


FIG. 2. (a) Normalized PL spectra of Mg-doped AlN nanowires with different Mg-cell temperatures and different growth rates measured at 20 K. A 193 nm ArF excimer laser was used as the excitation source. (b) Power dependent PL spectra of sample E at 20 K; inset: ratio of peak intensity of Mg-acceptor peak to that of band-edge peak versus power at 20 K.

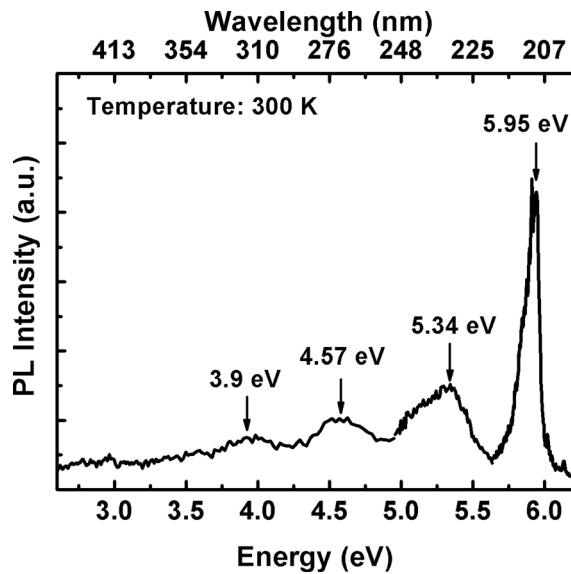


FIG. 3. Room temperature PL spectrum of sample E. A 197 nm frequency-quadrupled Ti-sapphire laser was used as the excitation source.

suggested that the observed red shift is likely a combination of band gap renormalization²⁵ and laser induced heating effect. This effect has been observed in GaN nano-particles²⁶ and also in GaN/AlN quantum dots.²⁷

It is observed from the low temperature PL spectra of Fig. 2(a) that the low energy peak, P_L , is quite broad. To investigate this peak more closely, the PL spectrum was measured at room temperature using a frequency-quadrupled Ti-sapphire laser with an emission wavelength at 197 nm, 76 MHz repetition rate, and an average optical power of ~ 1 mW as the excitation source. The room temperature PL spectrum of sample E is presented in Fig. 3. In addition to the band-edge peak at 5.95 eV, three other peaks were observed at 5.34 eV, 4.57 eV, and 3.9 eV. The peak at 5.34 eV can be identified as the Mg-acceptor related transition (the energy separation of the band-edge peak and the peak at 5.34 eV is 0.61 eV). The emission peaks at 4.57 eV and at 3.9 eV are attributed to the DAP transitions. The transition involving a deep donor and Mg-acceptor energy level is responsible for the peak at 4.57 eV whereas the peak at 3.9 eV is due to the transition involving a shallow donor and a deep acceptor. Such transitions were also observed in Mg-doped AlN epilayers.²¹

The temperature dependent PL properties have been investigated for the highly doped AlN sample under an

excitation power of 5 mW using the 193 nm ArF excimer laser as the excitation source. As the temperature increases, both peaks undergo a red shift. This is consistent with the band gap narrowing with temperature. The evolution of the peak energy with temperature is presented in Fig. 4(a). The temperature dependent band-gap change can be explained by the Varshni's equation,²⁸ $E_g(T) = E_g(0) - \alpha T^2/(\beta + T)$, shown as the solid line in Fig. 4(a), with the following parameters: $E_g(0) = 6.05$ eV, $\alpha = 1.8$ meV/K, and $\beta = 1462$ K. These values agree well with the previously reported values of AlN in this temperature range.²⁹ The evolution of the Mg-acceptor peak with temperature has also been studied. The integrated PL intensity as a function of inverse temperature is plotted in Fig. 4(b). The solid line is the least square fit of the experimental data with the equation $I_{emi} = I_0/(1 + a \exp(-E_0/KT))$, where I_{emi} denotes the integrated PL intensity at various temperatures, I_0 represents the integrated PL intensity at 0 K, and E_0 is the activation energy. The derived activation energy is ~ 80 meV, suggesting that the Mg-related transition is due to the DAP transition involving a Mg-acceptor energy level and a shallow donor. This activation energy is also comparable to the values (~ 60 meV) reported for AlN epilayers.²

We have subsequently investigated p-type conductivity by measuring the temperature-dependent current-voltage (I-V) characteristics of large area AlN:Mg nanowire arrays. The device structure (sample F) is schematically shown in Fig. 5(a), which consists of GaN/InGaN tunnel junction³⁰ grown on heavily n-doped Si substrate, a 90 nm thick AlN:Mg section followed by a 10 nm AlGaIn contact layer. The growth condition of AlN:Mg section is similar to that of sample E. The tunnel junction was designed to facilitate the carrier transport from the n-Si substrate to the p-AlN layer. To subtract the resistance associated with the substrate, tunnel junction, and contact region, another identical structure (sample F') but without the AlN:Mg section was fabricated. The difference in resistivity of these two structures can provide a reasonable estimation of the AlN:Mg nanowire resistance. The nanowires were first spin coated with polyimide. Ti/Au (20 nm/100 nm) and Ni/Au (50 nm/100 nm) were then deposited as the bottom and top contacts, respectively. The contacts were annealed in N_2 ambient at 500 °C for 1 min. The I-V characteristics were measured in the temperature range of 298–573 K and the resistance is calculated by the slope of the I-V curve in the forward bias region. The variation of AlN:Mg resistivity with inverse temperature is

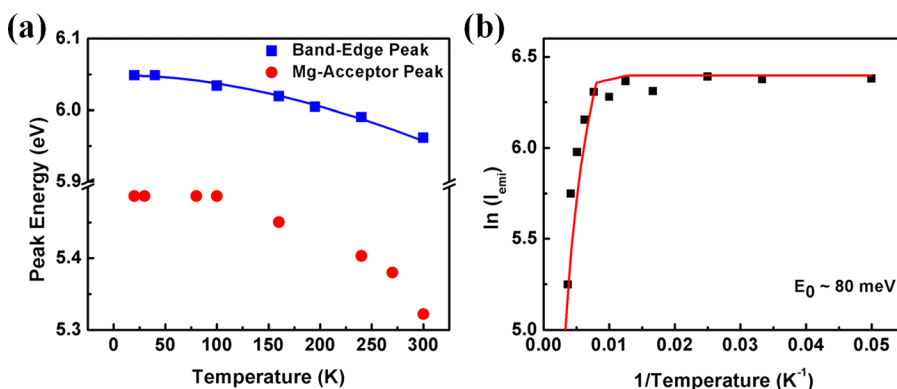


FIG. 4. (a) Peak energy variation with temperature for band-edge and Mg-acceptor peaks of sample E. The solid line is the calculation by the Varshni's equation. (b) Integrated PL intensity versus inverse temperature plot for the Mg-acceptor peak. The solid line is the least square fit of the experimental data with the equation, $I_{emi} = I_0/(1 + a \exp(-E_0/KT))$.

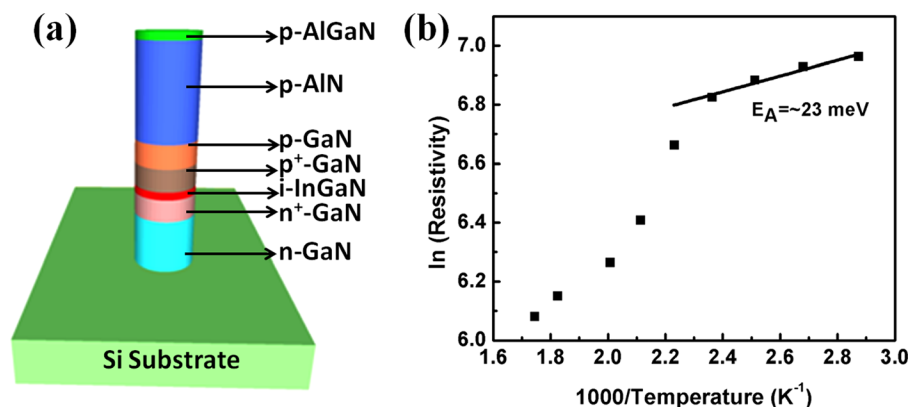


FIG. 5. (a) Schematic illustration of the structure to measure the resistivity of AlN:Mg nanowires; (b) Resistivity versus inverse temperature plot for AlN:Mg segment of sample F.

plotted in Fig. 5(b), which clearly reveals the presence of more than one activation energy. To discern the mechanism responsible for conduction at different temperature regions, the calculated resistivity is fitted by the equation, $\rho(T) = \rho_0 \exp(E_A/kT)$, where E_A is the thermal activation energy of resistivity. E_A is derived to be ~ 23 meV for the AlN:Mg segment. A similar activation energy (~ 50 meV) was also measured for AlN nanowires with reduced Mg dopant incorporation. Such an unusual low activation energy, compared to the Mg-acceptor energy level (~ 600 meV), suggests that the hole transport mechanism is mainly governed by hopping and/or impurity band transitions.^{31,32} In the hopping conduction, carriers hop from one localized state to another; the localized states could be at the same or at different energy levels. It is observed in Fig. 5(b) that the experimental data and the fitting curve follow each other closely in the temperature range of 300 K–450 K and there is a deviation in the higher temperature range. This deviation suggests that at higher temperatures the thermal activation of carriers starts to play a role and, at a sufficiently high temperature, thermal activation would be the dominating hole transport mechanism. This phenomenon has also been observed for $\text{Al}_{0.7}\text{Ga}_{0.3}\text{N}$,³¹ InGaN,³³ and GaN.³² With the room temperature resistivity value of $697 \Omega\text{-cm}$ and assuming an upper boundary of hole hopping mobility of $1 \text{ cm}^2/\text{V}\cdot\text{s}$,³⁴ the room temperature hole concentration of the AlN:Mg segment of sample F is found to be on the order of 10^{16} cm^{-3} , which is orders of magnitude higher than previously reported AlN:Mg epilayers.³⁴ The excellent p-type conductivity of AlN:Mg nanowires can be partly attributed to the drastically reduced nitrogen-vacancy related defects during the growth of nanowire structures under nitrogen-rich conditions as well as the enhanced dopant incorporation in nanowire structures.^{16,22}

In summary, we have investigated the optical and electrical properties of Mg-doped AlN nanowires. We have demonstrated that by optimizing the growth conditions, Mg-dopant incorporation in AlN nanowires can be significantly enhanced. Detailed studies further suggest that the hopping conduction dominates the carrier transport at room temperature, and the free hole concentration is estimated on the order of 10^{16} cm^{-3} .

This work was supported by the Natural Sciences and Engineering Research Council of Canada (NSERC) and U.S. Army Research Office under Grant No. W911NF-12-1-0477. Part of the work was performed in the McGill University

Micro Fabrication Facility. The authors wish to thank Dr. Qi Wang for useful discussions and help with some of the measurements. Work at TTU was supported by NSF (Grant No. ECCS-1402886). H. X. Jiang and J. Y. Lin are grateful to the AT&T Foundation for the support of Ed Whitacre and Linda Whitacre endowed chairs.

- ¹K.-T. Kenry, K. Yong, and S. F. Yu, *J. Mater. Sci.* **47**, 5341 (2012).
- ²K. B. Nam, M. L. Nakarmi, J. Li, J. Y. Lin, and H. X. Jiang, *Appl. Phys. Lett.* **83**, 878 (2003).
- ³K. Irmscher, T. Schulz, M. Albrecht, C. Hartmann, J. Wollweber, and R. Fornari, *Physica B: Condens. Matter* **401–402**, 323 (2007).
- ⁴B. N. Pantha, R. Dahal, M. L. Nakarmi, N. Nepal, J. Li, J. Y. Lin, H. X. Jiang, Q. S. Paduano, and D. Weyburne, *Appl. Phys. Lett.* **90**, 241101 (2007).
- ⁵M. L. Nakarmi, N. Nepal, J. Y. Lin, and H. X. Jiang, *Appl. Phys. Lett.* **94**, 091903 (2009).
- ⁶F. Glas, *Phys. Rev. B* **74**, 121302R (2006).
- ⁷S. Zhao, M. G. Kibria, Q. Wang, H. P. T. Nguyen, and Z. Mi, *Nanoscale* **5**, 5283 (2013).
- ⁸H. Hu, Z. Wu, W. Zhang, H. Li, R. Zhuo, D. Yan, J. Wang, and P. Yan, *J. Alloys Compd.* **624**, 241 (2015).
- ⁹Y. Y. Hui, J. Ye, R. Lortz, K. S. Teng, and S. P. Lau, *Phys. Status Solidi A* **209**, 1988 (2012).
- ¹⁰M. Qin, Y. Shang, X. Wang, and G. Zhang, *Sci. China: Technol. Sci.* **58**, 832–841 (2015).
- ¹¹Z.-K. Tang, L.-L. Wang, L.-M. Tang, X.-F. Li, W.-Z. Xiao, L. Xu, and L.-H. Zhao, *Phys. Status Solidi B* **249**, 185 (2012).
- ¹²Q. Wu, N. Liu, Y. Zhang, W. Qian, X. Wang, and Z. Hu, *J. Mater. Chem. C* **3**, 1113 (2015).
- ¹³Y. Xu, B. Yao, D. Liu, W. Lei, P. Zhu, Q. Cui, and G. Zou, *CrystEngComm* **15**, 3271 (2013).
- ¹⁴Y.-B. Tang, X.-H. Bo, J. Xu, Y.-L. Cao, Z.-H. Chen, H.-S. Song, C.-P. Liu, T.-F. Hung, W.-J. Zhang, H.-M. Cheng, I. Bello, S.-T. Lee, and C.-S. Lee, *ACS Nano* **5**, 3591 (2011).
- ¹⁵Q. Wang, S. Zhao, A. T. Connie, I. Shih, Z. Mi, T. Gonzalez, M. P. Andrews, X. Z. Du, J. Y. Lin, and H. X. Jiang, *Appl. Phys. Lett.* **104**, 223107 (2014).
- ¹⁶S. Zhao, A. T. Connie, M. H. Dastjerdi, X. H. Kong, Q. Wang, M. Djavid, S. Sadaf, X. D. Liu, I. Shih, H. Guo, and Z. Mi, *Sci. Rep.* **5**, 8332 (2015).
- ¹⁷Q. Wang, H. P. T. Nguyen, K. Cui, and Z. Mi, *Appl. Phys. Lett.* **101**, 043115 (2012).
- ¹⁸Q. Wang, A. T. Connie, H. P. T. Nguyen, M. G. Kibria, S. Zhao, S. Sharif, I. Shih, and Z. Mi, *Nanotechnology* **24**, 345201 (2013).
- ¹⁹K. B. Nam, M. L. Nakarmi, J. Y. Lin, and H. X. Jiang, *Appl. Phys. Lett.* **86**, 222108 (2005).
- ²⁰N. Nepal, K. B. Nam, M. L. Nakarmi, J. Y. Lin, H. X. Jiang, J. M. Zavada, and R. G. Wilson, *Appl. Phys. Lett.* **84**, 1090 (2004).
- ²¹M. L. Nakarmi, N. Nepal, C. Ugolini, T. M. Altahtamouni, J. Y. Lin, and H. X. Jiang, *Appl. Phys. Lett.* **89**, 152120 (2006).
- ²²S. Zhao, B. H. Le, D. P. Liu, X. D. Liu, M. G. Kibria, T. Szkopek, H. Guo, and Z. Mi, *Nano Lett.* **13**, 5509 (2013).
- ²³U. Kaufmann, M. Kunzer, M. Maier, H. Obloh, A. Ramakrishnan, B. Santic, and P. Schlotter, *Appl. Phys. Lett.* **72**, 1326 (1998).
- ²⁴S. Zhao, X. Liu, and Z. Mi, *Appl. Phys. Lett.* **103**, 203113 (2013).
- ²⁵T. Nagai, T. J. Inagaki, and Y. Kanemitsu, *Appl. Phys. Lett.* **84**, 1284 (2004).

- ²⁶A. B. Slimane, A. Najar, R. Elafandy, D. P. San-Román-Alerigi, D. Anjum, T. K. Ng, and B. S. Ooi, *Nanoscale Res. Lett.* **8**, 342 (2013).
- ²⁷I. Aleksandrov and K. Zhuravlev, *Phys. Status Solidi C* **7**, 2230 (2010).
- ²⁸Y. P. Varshni, *Physica* **34**, 149 (1967).
- ²⁹T. Hanada, *Oxide and Nitride Semiconductors*, Advances in Materials Reserach Vol. 12 (Springer, Berlin, 2009).
- ³⁰S. Krishnamoorthy, F. Akyol, P. S. Park, and S. Rajan, *Appl. Phys. Lett.* **102**, 113503 (2013).
- ³¹T. Kinoshita, T. Obata, H. Yanagi, and S.-I. Inoue, *Appl. Phys. Lett.* **102**, 012105 (2013).
- ³²P. Kozodoy, H. Xing, S. P. DenBaars, U. K. Mishra, A. Saxler, R. Perrin, S. Elhamri, and W. C. Mitchel, *J. Appl. Phys.* **87**, 1832 (2000).
- ³³K. Kumakura, T. Makimoto, and N. Kobayashi, *J. Appl. Phys.* **93**, 3370 (2003).
- ³⁴Y. Taniyasu, M. Kasu, and T. Makimoto, *Nature* **441**, 325 (2006).